

**Quantum phase transitions and persistent currents in Josephson-junction ladders**

Minchul Lee

*Department of Physics, Seoul National University, Seoul 151-747, Korea  
and Department of Physics, Korea University, Seoul 136-701, Korea*

Mahn-Soo Choi\*

*Department of Physics, Korea University, Seoul 136-701, Korea*

M. Y. Choi

*Department of Physics, Seoul National University, Seoul 151-747, Korea  
and Korea Institute for Advanced Study, Seoul 130-012, Korea*

(Received 27 February 2003; published 6 October 2003)

In this work we study quantum phase transitions and persistent currents in capacitively coupled one-dimensional Josephson-junction arrays. We will focus particularly on the roles of excitonlike pairs in the strong-coupling limit in the presence of external gate charges and magnetic fluxes. We use the numerical density-matrix renormalization group method for the study in the full range of values of gate charge and magnetic flux. To clarify the various effects, we report the pair correlation functions and exciton densities as well as the persistent current.

DOI: 10.1103/PhysRevB.68.144506

PACS number(s): 74.50.+r, 67.40.Db, 73.23.Hk

**I. INTRODUCTION**

Systems of Josephson junctions between small superconducting grains have been attracting considerable interest for more than two decades. One of the main attractive features is that they exhibit manifestations of various phenomena in diverse fields of condensed-matter physics. A popular example in contemporary mesoscopic physics is the Coulomb-blockade effect and single-charge (electron or Cooper pair) tunneling.<sup>1,2</sup> Persistent current, another hot topic in mesoscopic physics, can also be embodied in Josephson-junction systems. Since the superconducting coherence is easily maintained over a macroscopic length scale, a “necklace” of Josephson junctions (i.e., a one-dimensional periodic array of Josephson junctions) may be a good testbed for persistent currents.<sup>3</sup> Moreover, charge fluctuations present in such systems may induce quantum phase transitions,<sup>4–8</sup> providing a prototype model for the noble many-body phenomena in strongly correlated electron systems.<sup>9</sup> Another important and appealing feature of the systems is the experimental tunability: They not only make mesoscopic devices on their own<sup>10,2</sup> but also allow us to test and understand otherwise very subtle points of interacting many-particle systems,<sup>9</sup> which is important from a fundamental point of view.

Here we consider a particular geometry of Josephson-junction systems: a ladder of two capacitively coupled one-dimensional (1D) Josephson-junction arrays. In the Coulomb-blockade regime, a single charge cannot tunnel across the junction since it is energetically unfavorable. Transport is therefore dominated by more complex elementary processes that involve several charge-tunneling events. For the particular type of coupling through large interarray capacitances, the relevant elementary process in the absence of the gate charge consists of cotunneling of bound pairs of excess and deficit charges, which we call “particles” (excess charges) and “holes” (deficit charges), respectively.<sup>11</sup> It was

first demonstrated on capacitively coupled normal-metal tunneling junctions<sup>12,13</sup> and later on superconducting junction arrays.<sup>14,15</sup> In the presence of gate voltage applied between the electrode islands and substrate, the particle-hole symmetry is broken and the particle-hole pair no longer makes the lowest charging-energy configuration. For example, when the particle-hole symmetry is broken maximally (corresponding to the gate charge given by one-half of the elementary charge  $2e$ ), the transport is governed by cotunneling of particle-void pairs (with the *void* denoting the absence of any excess or deficit Cooper pair).<sup>14</sup> It is noted that these particle-hole pairs or particle-void pairs are reminiscent of *excitons*—i.e., bound states of a band electron and a hole—in solids. In the previous work,<sup>14</sup> quantum phase transitions induced by the cotunneling of particle-hole pairs and particle-void pairs near the particle-hole symmetry line and maximal-frustration line, respectively, have been studied by means of perturbative methods. However, the properties of the transport or phase transitions in between have not been studied.

The effects of an external magnetic flux threading the loop of a ladder of two capacitively coupled Josephson-junction necklaces (CCJJN's) (see Fig. 1) are even more sophisticated since the objects involved in the persistent current are not single charges. Unlike most studies of the persistent current [or, equivalently, the underlying Aharonov-Bohm (AB) effect], which focus on single-charged particles, recent researches into a nanostructure with nonsimply connected geometry have demonstrated<sup>17</sup> that excitons can contribute to persistent currents, in spite of their charge neutrality. The nonvanishing persistent currents in the system is attributed to the finite probability of breaking and recombination of an exciton via intermediate single-particle and -hole states. It is thus quite intriguing to investigate persistent currents in CCJJN's, where cotunneling of the particles and holes of Cooper pairs dominates the transport phenomena. Additional advantage of the CCJJN's is that the particle-

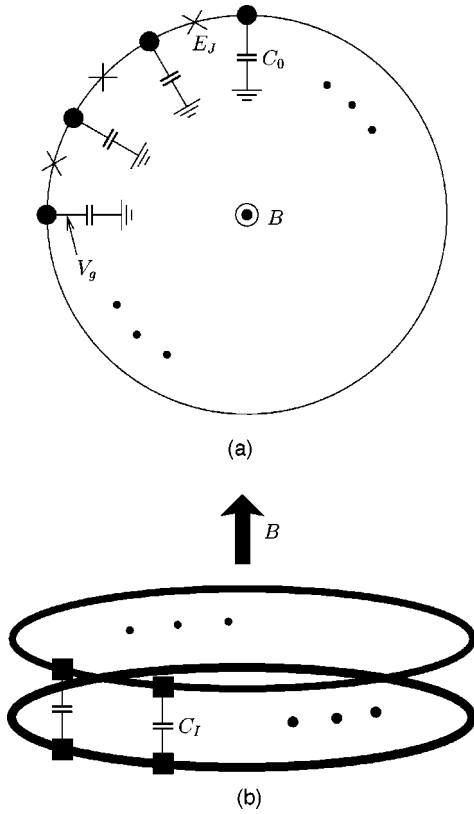


FIG. 1. Schematic diagrams of (a) a single Josephson-junction necklace (from above) and (b) two capacitively coupled necklaces (from the diagonal direction). In (b) each thick ring represents the single necklace depicted in (a).

hole or particle-void pairs are stable while the excitons in semiconductor nanorings usually have a finite and short lifetime. Notice further that the CCJN's are already within the reach of experimental realization.<sup>15</sup>

In this work we study quantum phase transitions and persistent currents in a ladder of CCJN's. We focus particularly on the roles of “excitons” in the presence of the charge frustration due to an external gate voltage and the magnetic frustration due to an external magnetic flux threading the necklaces. We use the numerical density-matrix renormalization group (DMRG) method<sup>18</sup> to probe the full ranges of gate charge and magnetic flux. Although we are mainly interested in the strong-coupling limit, we will consider for comparison both the two limiting cases: decoupled and strongly coupled cases. In the limit of strong coupling, we identify two different superfluid phases, characterized by condensation of either particle-hole pairs or particle-void pairs, depending on the gate charge. In order to disclose the properties of the superfluid phases and the formation of excitons explicitly, we measure the pair correlation function and exciton density. The behavior of the persistent current calculated for small systems reveals the transport via the separation and recombination process for small Josephson energies. At larger Josephson energies, however, the transport is governed by a mixing of low-lying charge states with higher-energy states. Finally, we propose an experimentally realizable system to demonstrate the cotunneling process of excitons. The

intermediate-coupling regime is also interesting and more feasible experimentally.<sup>15</sup> Unfortunately, however, a numerical DMRG study in this case is beyond current computing power, requiring far more memory than available. We thus leave the intermediate region for future study.

The remaining part of this paper is organized as follows: In Sec. II we first describe the model Hamiltonians and discuss qualitatively the relevant low-energy charge states. Quantum phase transitions in a single Josephson-junction necklace and capacitively coupled Josephson-junction necklaces are examined in Sec. III. Section IV is devoted to the investigation of the persistent currents in the system, revealing the AB effect of excitons. Finally, we summarize the main results in Sec. V.

## II. MODEL

We consider two 1D periodic arrays, which we call *necklaces*, of  $N$  superconducting grains as shown in Fig. 1. Any two nearest-neighboring grains on one necklace form a Josephson junction of coupling strength  $E_J$ . The two necklaces are coupled with each other via capacitance  $C_I$  between corresponding grains to form a “ladder.” Uniform gate voltage  $V_g$  is applied to each grain through its self-capacitance  $C_0$ , inducing gate charge  $Q = C_0 V_g$  on each grain. For convenience, we measure the charge in units of  $2e$  and write  $Q \equiv 2en_g$ . In addition, a transverse magnetic flux threads each necklace. Such a system is described by the Hamiltonian

$$\mathcal{H} = 2e^2 \sum_{lx, l'x'} [n_x^l - n_g] C_{lx, l'x'}^{-1} [n_{x'}^{l'} - n_g] - E_J \sum_{lx} \cos(\phi_x^l - \phi_{x+1}^l - A_x), \quad (1)$$

where the number  $n_x^l$  of Cooper pairs and the phase  $\phi_x^l$  of the superconducting order parameter at site  $x$  on the  $l$ th necklace ( $l=1,2$ ) are quantum mechanically conjugate variables:  $[n_x^l, \phi_{x'}^{l'}] = i\delta_{l,l'}\delta_{x,x'}$ . The bond angle  $A_x$  is given by the line integral of the vector potential  $\mathbf{A}$  introduced by the applied magnetic field:

$$A_x = \frac{2\pi}{\Phi_0} \int_x^{x+1} d\mathbf{l} \cdot \mathbf{A} = \frac{2\pi f}{N}, \quad (2)$$

where  $f$  denotes the total flux in units of the flux quantum  $\Phi_0 \equiv 2\pi\hbar c/2e$ . Assuming that junction capacitances are negligible, we write the capacitance matrix  $C_{lx, l'x'}$  in the form<sup>16</sup>

$$C_{lx, l'x'} = [C_0\delta_{l,l'} + C_I(2\delta_{l,l'} - 1)]\delta_{x,x'} \equiv C_{ll'}\delta_{x,x'} \quad (3)$$

and also define charging energy scales  $E_0 \equiv e^2/2C_0$  and  $E_I \equiv e^2/2C_I$ , associated with the corresponding capacitances. Notice, that when  $n_g = 0$  the Hamiltonian in Eq. (1), is symmetric with respect to the particlelike (excess Cooper pairs) excitations and holelike (deficit pairs) ones. On the other hand, charges on each grain are maximally frustrated when  $n_g = 1/2$ . For later use, we thus name the lines corresponding

to  $n_g=0$  and  $n_g=1/2$  the particle-hole symmetry line and maximal-frustration line, respectively, in the phase diagram.

For the DMRG analysis, we represent the Hamiltonian in Eq. (1) in the boson number basis. Based on the commutation relation between the number  $n_x^l$  and phase  $\phi_x^l$ , we identify the boson creation operator  $b_x^{l\dagger}$  at site  $x$  on necklace  $l$  with  $e^{i\phi_x^l}$ . In terms of the boson operators, we thus obtain the Bose-Hubbard Hamiltonian

$$\mathcal{H}_{BH} = \frac{8E_0}{2} \sum_{ll'x} n_x^l C_0 C_{ll'}^{-1} n_{l'}^{l'} - 8E_0(n_g + \bar{n}) \sum_{lx} n_x^l - \frac{E_J}{2\bar{n}} \sum_{lx} (e^{-2\pi if/N} b_x^{l\dagger} b_{x+1}^l + \text{H.c.}), \quad (4)$$

where  $\bar{n}$  is the average boson number per site. Note that in the quantum phase model the Josephson energy term is independent of the number fluctuations, while the corresponding (hopping) term is not in the Bose-Hubbard model. To alleviate the effects of number fluctuations in the Bose-Hubbard model, we consider the case that the average boson number  $\bar{n}$  per site is large.<sup>19</sup> Throughout this study we set  $\bar{n}$  to be 10 000.

Capacitive coupling between necklaces drastically affects the low-lying charge excitations, especially in the strong-coupling regime. To examine the charge configurations in the low-lying states, it is convenient to rewrite the charging energy part in the Hamiltonian (4):

$$\mathcal{H}_{BH} = U_0 \sum_x (n_x^+ - 2n_g)^2 + V_0 \sum_x (n_x^-)^2 - \frac{E_J}{2\bar{n}} \sum_{lx} (e^{-2\pi if/N} b_x^{l\dagger} b_{x+1}^l + \text{H.c.}), \quad (5)$$

where we have defined new energy scales  $U_0 \equiv 2E_0$  and  $V_0 \equiv 2E_0/(1+2C_I/C_0)$  and charge variables  $n_x^{\pm} \equiv (n_{1,x} - \bar{n}) \pm (n_{2,x} - \bar{n})$ . Note that  $n_x^+$  represents the total number of (excess) Cooper pairs on the  $x$ th rung of the ladder. In the regime of concern ( $C_I \gg C_0$ , i.e.,  $E_J \ll E_0$ ), we have  $U_0 \gg V_0$  and  $U_0 \gg E_J$ , and the charge configurations satisfying  $n_x^+ - 2n_g \approx 0$  are thus strongly favored. In such a charge configuration  $n_x^-/2$  corresponds to the number of excitons (particle-hole or particle-void pairs; see below).

The representation in Eq. (5) of the Hamiltonian allows us to distinguish clearly the two interesting regions from each other: near the particle-hole symmetry line ( $n_g=0$ ) and near the maximal-frustration line ( $n_g=1/2$ ), as one can observe from the energy spectra of the charging energy part illustrated in Figs. 2 and 3 for the two regimes, respectively. Near the maximal-frustration line, the charge configurations that do not satisfy the condition  $n_x^+ = 1$  (for all  $x$ ) have a huge excitation gap of the order of  $E_0$ . Furthermore, the ground states of the charging energy part, separated from the excited states by a gap of the order of  $E_J$ , have twofold degeneracy for each  $x$ , corresponding to  $n_x^- = \pm 1$ . Near the particle-hole symmetry line, on the other hand, low-energy charge con-

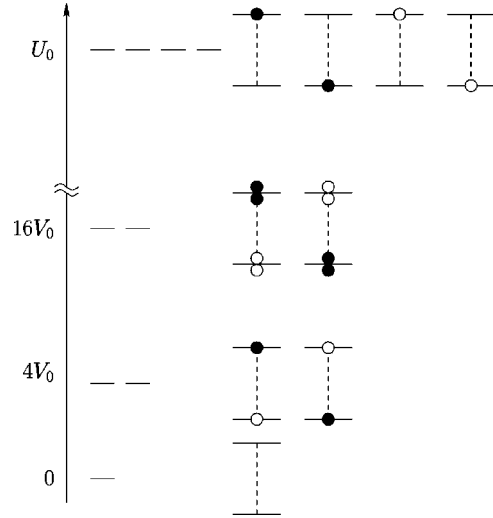


FIG. 2. Energy levels of the charging energy part in Eq. (5) and corresponding charge configurations near the particle-hole symmetry line. Solid and open circles denote particles and holes, respectively; paired (upper and lower) solid lines represent the two coupled arrays, the couplings between which are illustrated by the dashed lines. The low-lying energy levels satisfying  $n_x^+ = 0$  are well separated by a large amount of energy (of the order of  $E_0$ ) from those with  $n_x^+ \neq 0$ .

figurations should satisfy the condition  $n_x^+ = 0$  for all  $x$ . Unlike the former case, the ground state of the charging energy is nondegenerate and forms a Mott insulator characterized by  $n_{1,x} = n_{2,x} = 0$  for all  $x$ . As  $E_J$  is turned on, the ground state is

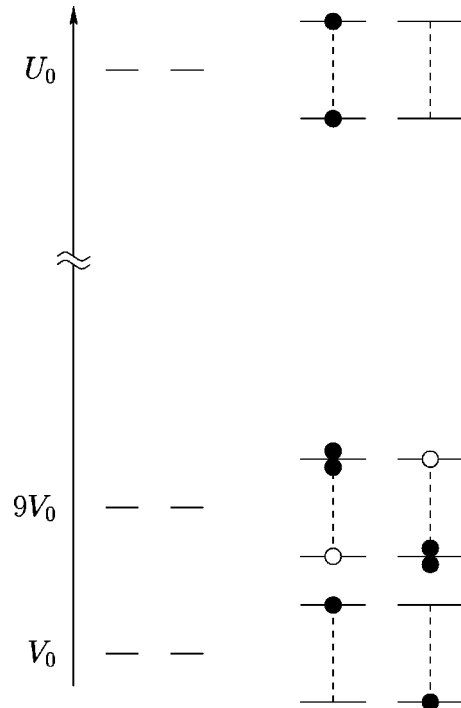


FIG. 3. Energy levels and corresponding charge configurations near the maximal-frustration line. Note that the ground state is twofold degenerate per site.

mixed with the states with  $n_x^- = \pm 2$ . In the intermediate region ( $0 < n_g < 1/2$ ), these two kinds of energy spectra are interleaved to form a complex shape of the energy levels.

### III. QUANTUM PHASE TRANSITIONS

The competition between charge order and phase coherence gives rise to quantum fluctuations and quantum phase transitions at zero temperature. For large charging energy ( $E_0 \gg E_J$ ), the bosons become localized and the system is in the Mott insulator phase with integer density. On the contrary, for large hopping energy or Josephson energy ( $E_J \gg E_0$ ), coherence of the phases  $\phi_x$  dominates over the system and a superfluid (SF) region with delocalized bosons is observed. The properties and universality classes of the phase transitions, however, depend strongly on the coupling strength  $C_I/C_0$  as well as the chemical potential  $\mu \equiv 8E_0(n_g + \bar{n})$ . The charge frustration  $n_g$  may be restricted to the range  $[1, 1/2]$  since the Hamiltonian in Eq. (5) is periodic in  $n_g$  with period unity and has reflection symmetry about the  $n_g = 1$  (or any integer) line. In the following we investigate two limiting cases: the decoupled case ( $C_I = 0$ ) and the strongly coupled one ( $C_I \gg C_0$ ).

#### A. Single Josephson-junction necklace

The phase transition in a single Josephson-junction array has been studied quite extensively and it has been found that its nature depends crucially on the gate voltage. In the presence of nonzero gate voltage ( $n_g \neq 0$ ), the density of the system changes as the phase boundary is crossed from an incompressible insulator to a compressible superfluid. The transition can thus be located at the point where in the thermodynamic limit the density of the ground state becomes different from one of the insulator ground state as the Josephson energy is increased. On the other hand, in the particle-hole symmetry line ( $n_g = 0$ ), the density remains an integer at the phase transition. Therefore, in this case the phase boundary is determined by the single-particle excitation gap. This is possible because in the superfluid phase the ground state is a superposition of states with different boson numbers; the energy gap between the ground state and states with additional particles, which is finite in the insulating phase, vanishes in the superfluid phase.

Since the Hamiltonian conserves total charge number, the DMRG algorithm can be set up to target states with given total excess number  $M$  of bosons. We thus obtain the phase diagram of the system by comparing energies of the ground states with different boson numbers: the energy  $E_{M=0}$  of the insulator ground state with zero excess boson density ( $\langle n_x \rangle = \bar{n}$ ) and the energy  $E_{M=1}$  of the eigenstate with an additional particle upon the ground state. Through the linear extrapolation of the energy gap  $E_{M=1} - E_{M=0}$  for finite system size  $N = 64, 128$ , and  $256$ , we have estimated the gap in the thermodynamic limit and located the phase boundary at the point where the gap is zero. For high numerical accuracy and access to large systems, the finite-size DMRG algorithm and open boundary conditions have been used. During the DMRG process, the boson number at each site is truncated to

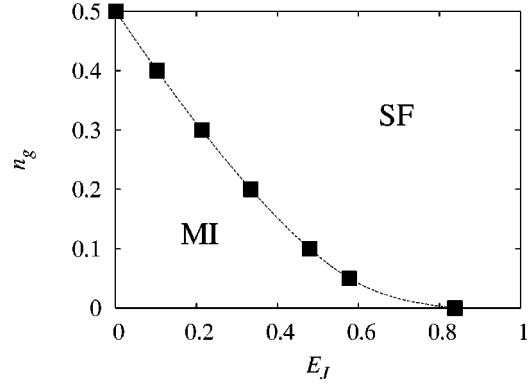


FIG. 4. Phase diagram for a single 1D Josephson array. The phase boundary separates the Mott insulator (MI) with zero excess Cooper pair density from the superfluid phase (SF). The Josephson energy  $E_J$  is expressed in units of  $8E_0$  and the error bars in the  $E_J$  direction (for given  $n_g$ ) are smaller than the square symbols. The line is merely a guide to the eye.

be less than 6 and the discarded weight is set to be less than  $10^{-6}$ , giving rise to negligible errors in the gap energy.<sup>20</sup> The magnetic frustration  $f$  is set equal to zero because it can be gauged away and becomes irrelevant in the thermodynamic limit.

Figure 4 displays the resulting phase diagram for the quantum phase model on the  $E_J$ - $n_g$  plane in the range  $0 \leq n_g \leq 1/2$  and  $0 \leq E_J \leq 8E_0$ . For convenience, here and in all subsequent figures, the energy is expressed in units of  $8E_0$ . The phase diagram, where the Mott insulator region with zero excess boson density is separated from the compressible superfluid, is in good agreement with those obtained via the perturbative expansion<sup>21</sup> and the quantum Monte Carlo method.<sup>22</sup> On the particle-hole symmetry line the quantum phase model is mapped exactly to the (1+1)-dimensional XY model, predicting a Beresenski-Kousterlitz-Thouless (BKT) transition<sup>23</sup> driven purely by phase fluctuations. The sharp-pointed shape of the insulating region near the symmetry line reflects the slowness in closing the energy gap in the BKT transition.<sup>20</sup> In case that the particle-hole symmetry is broken (away from the symmetry line), no such slowness is found and the commensurate-incommensurate transition belongs to a universality class other than that of the XY model, with different critical exponents<sup>22</sup> and RG characteristics.<sup>24</sup>

#### B. Strongly coupled Josephson-junction necklaces

In the strong-coupling limit, the low-energy charging states relevant to the phase transition are the particle-hole pairs (with  $n_x^+ = 0$  and  $n_x^- = \pm 2$ ) and the particle-void pairs (with  $n_x^+ = 1$  and  $n_x^- = \pm 1$ ). For small hopping strength, these excitons are localized and the system is in the Mott insulator phase. As  $E_J$  increases, the phase boundary is crossed from the insulator to the superfluid which, in this case, originates from condensation of the excitons. Accordingly, as in the case of a single Josephson-junction necklace, the transition can be located as one tracks the energy taken to add an exciton to the insulator: At the phase boundary this

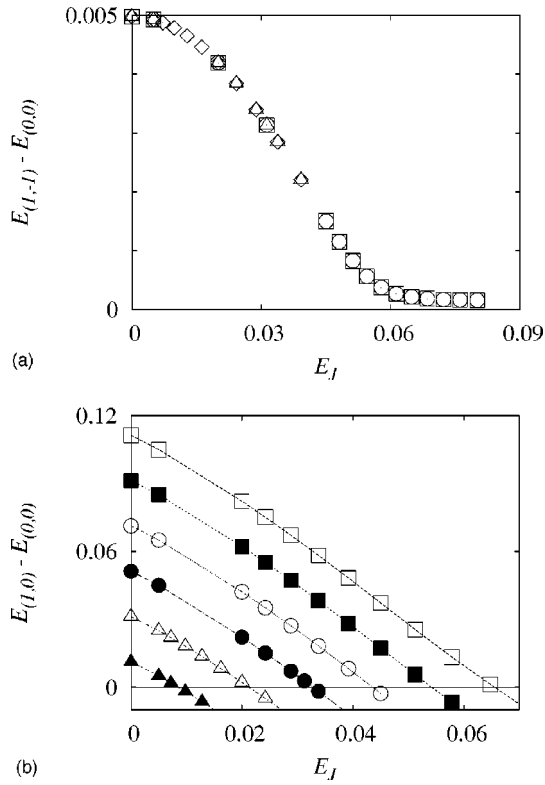


FIG. 5. Energy gaps (a)  $E_{(1,-1)} - E_{(0,0)}$  and (b)  $E_{(1,0)} - E_{(0,0)}$ . Both are taken for  $C_I/C_0 = 100$  at the system size  $N = 32$ . Each symbol corresponds to a different value of charge frustration: (a)  $n_g = 0$  ( $\square$ ), 0.1 ( $\circ$ ), 0.2 ( $\triangle$ ), and 0.24 ( $\diamond$ ); (b)  $n_g = 0.14$  ( $\square$ ), 0.16 ( $\blacksquare$ ), 0.18 ( $\circ$ ), 0.2 ( $\bullet$ ), 0.22 ( $\triangle$ ), and 0.24 ( $\blacktriangle$ ). The energies on both axes are expressed in units of  $8E_0$ .

energy vanishes in the thermodynamic limit. Which kind of exciton between the particle-hole pair and particle-void pair is relevant depends on the charge frustration  $n_g$ . Near the particle-hole symmetry line ( $n_g \approx 0$ ), the particle-hole pairs are energetically favorable and govern the phase transition. As  $n_g$  is increased and in the presence of Josephson tunneling, in contrast, the particle-void pairs begin to be dominant faster than the particle-hole pairs, which will be shown below.

In the DMRG procedure we have associated the target state with a pair of total excess boson numbers ( $M_1, M_2$ ) on the two arrays by utilizing boson number conservation. In order to locate the phase boundary, we have calculated the energy  $E_{(M_1, M_2)}$  of three kinds of eigenstate: the insulator ground state with  $(M_1, M_2) = (0, 0)$  and the states with additional particle-hole and particle-void pairs upon the ground state, labeled by  $(M_1, M_2) = (1, -1)$  and  $(1, 0)$ , respectively. We have extrapolated the energy gaps  $E_{(1,-1)} - E_{(0,0)}$  and  $E_{(1,0)} - E_{(0,0)}$  for finite system size  $N = 16, 32$ , and  $64$  to locate the transition points where the gaps vanish in the thermodynamic limit. As in the case of a single Josephson necklace, we have employed the finite-size DMRG algorithm, imposing open boundary conditions.

Figure 5 shows the energy gaps as functions of the Josephson energy at various charge frustrations in the system with  $C_I/C_0 = 100$  and  $N = 32$ . From Fig. 5(a) we observe

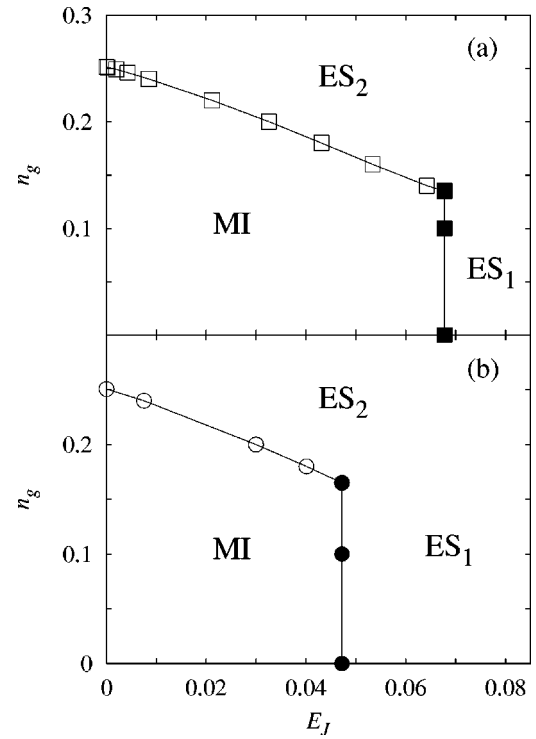


FIG. 6. Phase diagrams for strongly coupled 1D Josephson arrays for (a)  $C_I/C_0 = 100$  and (b)  $C_I/C_0 = 200$ . Displayed are the phase boundaries between the Mott insulator (MI) phase and the superfluid phase (ES<sub>1</sub> and ES<sub>2</sub>). Regions ES<sub>1</sub> and ES<sub>2</sub> in the superfluid phase are distinguished by the dominant transport mechanism (see the text). The transitions across the boundaries indicated by solid and open symbols are driven by the particle-hole pairs and particle-void pairs, respectively. The lines are merely guides to the eye.

that the excitation energy  $E_{(1,-1)} - E_{(0,0)}$  for different charge frustrations collapses into one curve, which also happens at other system sizes. This indicates that the critical Josephson energy at the transition driven by particle-hole pairs does not depend on  $n_g$ . On the other hand, the energy gap  $E_{(1,0)} - E_{(0,0)}$  decreases almost linearly with the increase of  $n_g$  and  $E_J$ , as shown in Fig. 5(b). The larger  $n_g$  is, the smaller the Josephson energy  $E_J$  at which the energy gap vanishes becomes. For  $n_g \geq 0.14$ , the critical value of  $E_J$  become even less than that for the particle-hole pairs.

The resulting phase diagrams for strongly coupled arrays with  $C_I/C_0 = 100$  and  $200$  are exhibited in Figs. 6(a) and 6(b), respectively. Based on the dominant transport mechanism, one can distinguish three regions in the superfluid phase: ES<sub>1</sub>, ES<sub>2</sub>, and SFUB. In region ES<sub>1</sub> the transport is driven mainly by the excitons of particle-hole pairs; in ES<sub>2</sub> it is driven by particle-void pairs. In region SFUB, on the other hand, single-particle processes dominate the transport in the system. Such a superfluid of unpaired bosons (SFUB) is to be observed at  $E_J/8E_0 \sim 1$ , far to the right from regions ES<sub>1</sub> and ES<sub>2</sub>, and not shown in the phase diagram given by Fig. 6. We note that different transport mechanisms take over dominant roles gradually as the control parameters are changed. Therefore, regions ES<sub>1</sub> and ES<sub>2</sub> in Fig. 6 should not correspond to truly distinct phases.

Previous studies of the mapping of the system at the particle-hole symmetry line to a (1+1)-dimensional system of classical vortices<sup>25,26</sup> insisted that the system is effectively described by a two-dimensional XY model and exhibits a BKT transition at the critical Josephson energy  $E_J/8E_0|_c = 4K_{BKT}^2(1 + \sqrt{1 + 2C_I/C_0})^{-2} \approx 2K_{BKT}^2(C_0/C_I)$ , where  $K_{BKT} \approx 0.748$  is the critical coupling strength for the standard XY model. Our data, though being unable to discern nature of the transition, show that the critical Josephson energy is inversely proportional to  $\sqrt{C_I/C_0}$  instead of  $C_I/C_0$ , apparently favoring against the BKT transition. This result is quite reasonable in view of the fact that the cotunneling process of particle-hole pairs via an intermediate virtual state happens with probability proportional to  $E_J^2/E_0E_I$ , leading to  $E_J/E_0|_c \propto \sqrt{C_I/C_0}$ . In addition, the nonzero charge frustration does not change the properties of the phase transition abruptly, in contrast to the case of a single array. Instead, the transition point as well as the qualitative properties is preserved up to  $n_g \approx 0.135$  for  $C_I/C_0 = 100$  and to  $n_g \approx 0.165$  for  $C_I/C_0 = 200$ ; there is no increase in the critical value of  $E_J$  as predicted in Ref. 14. Since our model neglects the junction capacitance on each necklace, for

$$n_g > n_g^* \equiv \frac{1}{4} \left( 1 + \frac{1}{1 + 2C_I/C_0} \right), \quad (6)$$

each site has twofold-degenerate ground states ( $n_x^+ = 1$  and  $n_x^- = \pm 1$ ) of the charging energy. Accordingly, the Josephson energy of any strength brings about charge fluctuations to drive the system into the superfluid phase. Indeed Fig. 6 shows that the MI phase ceases to exist for  $n_g > n_g^*$ , regardless of  $E_J$ . With nonzero junction capacitance, the degeneracy is expected to be broken, generating another insulating phase: the charge-density-wave (CDW) phase. A perturbative study<sup>14</sup> has found that as the Josephson energy is increased the system goes from the CDW insulator to the Luttinger liquid phase.

To witness the activity of the excitons in the phase transition, we have measured the pair correlation function defined to be

$$C_{pair} \equiv \frac{1}{N} \sum_x \langle (n_x^1 - \langle n_x^1 \rangle)(n_x^2 - \langle n_x^2 \rangle) \rangle \quad (7)$$

together with the exciton density  $P_0$  of the particle-hole pairs and  $P_{\pm 1}$  of the particle-void pairs:

$$P_0 \equiv \frac{1}{N} \sum_x \langle \delta_{n_x^1 + n_x^2, 0} - \delta_{n_x^1, 0} \delta_{n_x^2, 0} \rangle, \quad (8)$$

$$P_{n^+} \equiv \frac{1}{N} \sum_x \langle \delta_{n_x^1 + n_x^2, n^+} \rangle \quad (n^+ \neq 0). \quad (9)$$

The pair correlation function assumes zero if there is no correlation between the boson numbers on the two arrays; a particle-hole or particle-void pair at every site on the average contributes to  $C_{pair}$  by  $-1$  or  $-1/4$ .

Figure 7 shows that the pair correlation is negative and monotonically decreases with  $E_J$ , which indicates that larger

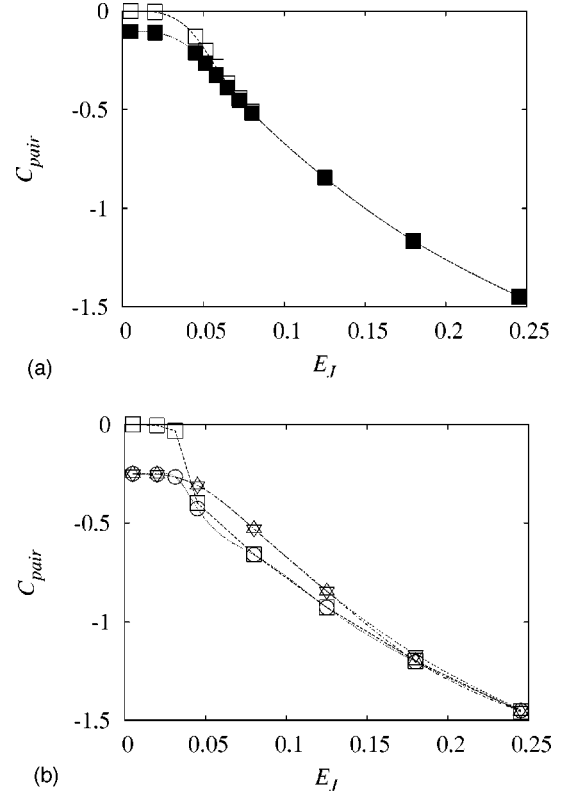


FIG. 7. Pair correlation  $C_{pair}$  vs the Josephson energy. (a) For  $n_g = 0$ , the pair correlation functions in the insulator ground state (open symbols) and in the state with one particle-hole pair added upon the ground state (solid symbols) are plotted. (b) shows the correlations in the ground state in the presence of the gate voltage  $n_g = 0.2$  ( $\square$ ),  $0.3$  ( $\circ$ ),  $0.4$  ( $\triangle$ ), and  $0.5$  ( $\nabla$ ). Here we set  $C_I/C_0 = 100$  and the system size  $N = 8$ , and lines are guides to the eye.

hopping strength makes more excitons come into the system. For  $n_g = 0$  [see Fig. 7(a)], the two pair correlation functions—one for the insulator ground state and the other for the state with an additional particle-hole pair—approach each other and collapse at  $E_J/8E_0 \geq 0.07$ , giving further evidence for the condensation of excitons. For  $n_g = 0.2$ , the correlation changes abruptly at the phase transition, as shown in Fig. 7(b). For  $n_g \geq 0.3$ , we have  $C_{pair} \approx -1/4$  for small values of  $E_J$ , which reflects the contribution of particle-void pairs. Although the correlations for  $n_g \geq 0.3$  become similar at large values of  $E_J$ , they do not coincide at intermediate values, implying a difference in the history of pair generation.

The behavior of the exciton density with  $E_J$ , displayed in Fig. 8, manifests more clearly the formation of excitons. The particle-hole pair density  $P_0$  grows with  $E_J$  [see Fig. 8(a)], except for the case of  $n_g = 0$  and large  $E_J$ . On the other hand, Fig. 8(b) shows that the density  $P_1$  of the particle-void pairs with  $n_x^1 + n_x^2 = 1$  has two kinds of tendencies: For  $n_g < n_g^*$  the density  $P_1$  increases with  $E_J$ ; otherwise, it decreases. The steep changes in both densities  $P_0$  and  $P_1$  happen when the total excess boson number  $M = M_1 + M_2$  of the ground state is altered. Such behaviors of  $P_0$  and  $P_1$  reveal that more than one kind of excitons proliferates in the system

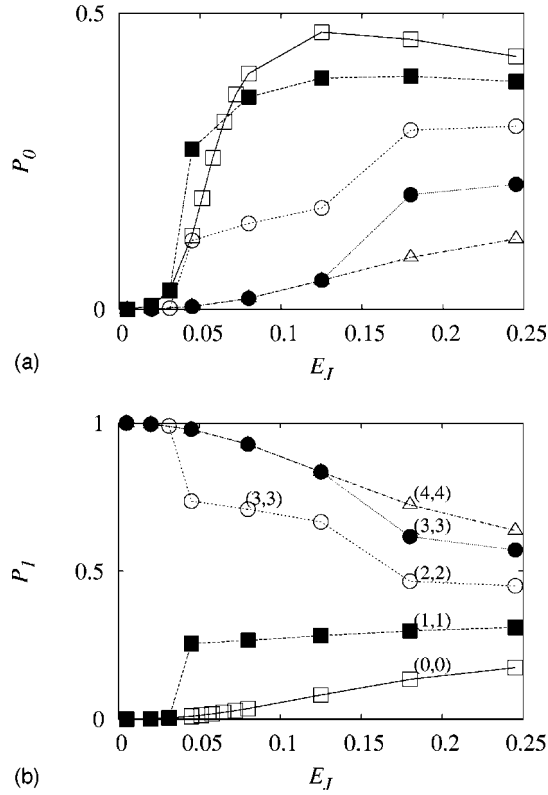


FIG. 8. Exciton densities (a)  $P_0$  and (b)  $P_1$  vs the Josephson energy for gate voltage  $n_g=0$  ( $\square$ ), 0.2 ( $\blacksquare$ ), 0.3 ( $\circ$ ), 0.4 ( $\bullet$ ), and 0.5 ( $\triangle$ ). Other parameters are the same as those in Fig. 7. The pairs of numbers  $(M_1, M_2)$  represent the total excess boson numbers of the ground state at given parameters.

as  $E_J$  is increased beyond its critical value. With large  $E_J$ , the kinetic energy gain due to the Josephson tunneling term compensates for the charging energy gap between different kinds of excitons.

We close this section with a comment about the pair correlation in the limit  $E_J/8E_0 \gg 1$ , which is beyond our current computational power. Our data show no indication of the decrease of the pair correlation with  $E_J$  raised. However, when the Josephson energy is large enough for the single processes of unpaired particles to prevail, the pair correlation may eventually approach zero again.

#### IV. PERSISTENT CURRENT

In this section we consider the persistent current along the necklaces, induced by the threading external magnetic field. Since tunneling of Cooper pairs between necklaces is not permitted, the persistent current carried by each necklace is given by the derivative of the energy with respect to the magnetic flux  $f$  (Ref. 3):

$$I_l = \frac{e}{2\pi\hbar} \left\langle \frac{\partial \mathcal{H}}{\partial f} \right\rangle_l = -\frac{eE_J}{N\hbar} \text{Im} \langle e^{-2\pi i f / N} b_x^{l\dagger} b_{x+1}^l \rangle, \quad (10)$$

which is simply the supercurrent through the Josephson junctions. The current in the system is thus given by the imaginary part of  $\langle \exp[i(\phi_x^l - \phi_{x+1}^l - A_x)] \rangle$ , the real part of which

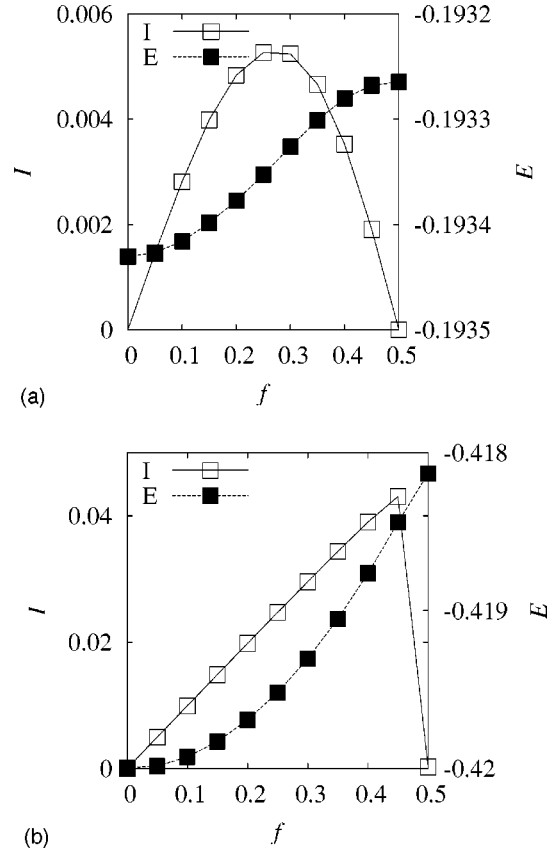


FIG. 9. Persistent current  $I$  and ground-state energy  $E$  as functions of the flux  $f$  in (a) the insulating phase ( $E_J/8E_0=0.64$ ) and (b) the superfluid phase ( $E_J/8E_0=1$ ) along the particle-hole symmetry line ( $n_g=0$ ).

describes the gauge-invariant phase correlation function between nearest-neighboring grains. Since the current is periodic in  $f$  with period unity and an odd function of the flux  $f$ , it is sufficient to calculate the current in the range  $f \in [0, 1/2]$ . As in the previous section, we focus on two extreme cases: the decoupled case ( $C_I=0$ ) and strongly coupled one ( $C_I/C_0 \gg 1$ ).

##### A. Single Josephson-junction necklace

We have calculated the persistent current in a finite-size system ( $N=40$ ) under periodic boundary conditions. The persistent current is evaluated in the ground state—namely, the lowest-energy state—which is found by varying the total excess boson number  $M$  at given  $n_g$  and  $E_J$ , and expressed in units of  $eE_J/N\hbar$  in all subsequent figures. Figures 9(a) and 9(b) show the dependence of the persistent current (in units of  $eE_J/N\hbar$ ) and of the ground-state energy (in units of  $8E_0$ ) on the flux  $f$  in both the insulating phase and superfluid phase, respectively, without the gate charge ( $n_g=0$ ). For small  $E_J$ , the current depends sinusoidally on  $f$ , whereas it has a sawtooth shape in the superfluid phase. Such behavior of the persistent current is well known in the two extreme one-dimensional electron models: In the tight-binding model with the lattice potential energy dominant over the kinetic energy, the single-particle energy is given by a cosine func-

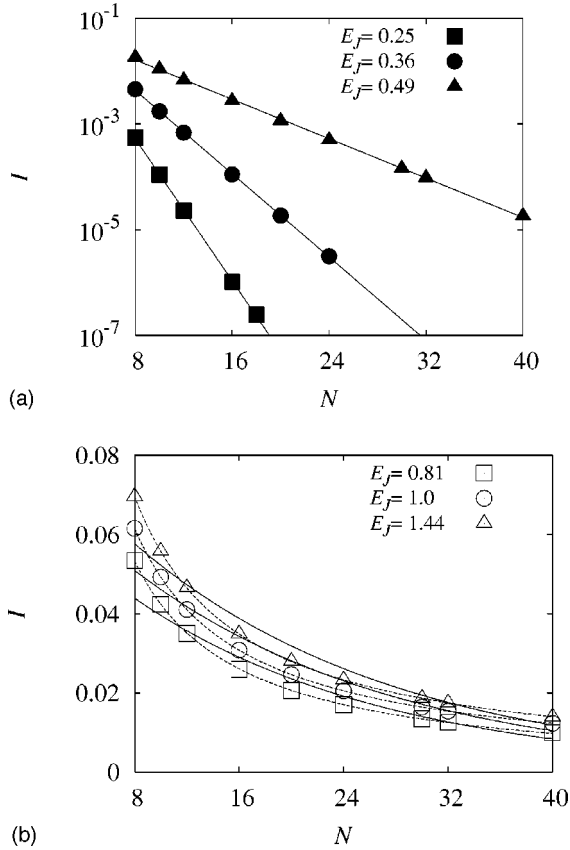


FIG. 10. Persistent current  $I$  vs the system size  $N$  in (a) the insulating phase [ $E_J=0.25$  (■),  $0.36$  (●), and  $0.49$  (▲) in units of  $8E_0$ ] and (b) the superfluid phase [ $E_J=0.81$  (□),  $1$  (○), and  $1.44$  (△) in units of  $8E_0$ ] along the particle-hole symmetry line ( $n_g=0$ ). Solid and dotted lines represent the exponential function  $ae^{-bN}$  and the algebraic function  $c/N$ , respectively, where the constants  $a$ ,  $b$ , and  $c$  are obtained via a fitting algorithm.

tion of the flux  $f$ , giving rise to a sinusoidal dependence of the current on  $f$ . On the other hand, the free-electron model on a ring, where the energy is quadratic in  $f$ , has the persistent current linear in  $f$  and of sawtooth shape. In our model Cooper pairs take the role of the electrons and in analogy we infer that the sawtooth dependence in the persistent current indicates the emergence of the superconductivity over the system, where the Cooper pairs can freely move around. Our data for the dependence of the current on the system size, shown in Fig. 10, also lead to the same interpretation: In the insulating phase the bosons are localized at sites so that the probability for a boson to circle around the ring and to return to its starting position is proportional to  $t^N$ , where  $t$  is the hopping probability between nearest neighbors. This gives a current decaying exponentially with system size  $N$  [see Fig. 10(a)]. On the other hand, in the superfluid phase the wave function of the boson is extended and the hopping probability over the system does not depend on the system size. Instead, since the energy itself is quadratic in the system size, the persistent current follows a power law with respect to the system size, as shown in Fig. 10(b). Hence our data for the persistent current are fully consistent with the phase transition explained in Sec. III A.

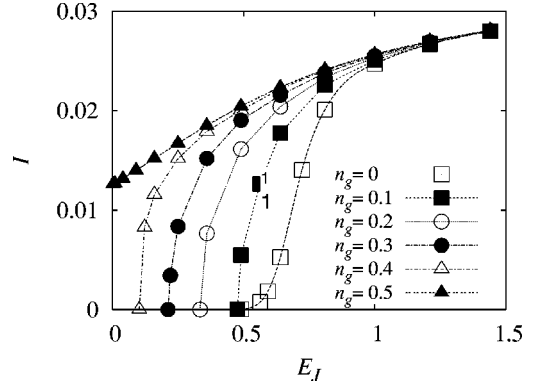


FIG. 11. Persistent current vs the Josephson energy for various gate voltages. In each case the current, scaled in units of  $eE_J/N\hbar$ , makes clear the contribution of the correlations between nearest-neighbor grains. All the currents are calculated at  $f=1/4$ .

We exhibit the dependence of the persistent current on the Josephson energy at  $f=1/4$  and various gate voltages in Fig. 11. The persistent current scaled by  $E_J$  is negligibly small in the insulating region, then rises rapidly near the transition point, and increases only marginally in the superfluid phase. For  $n_g=0$ , the current shows finite-size effects, gradually increasing quite before the transition point. On the contrary, in the presence of nonzero gate voltage, the current increases very sharply at the phase boundary even in the small-size system, which is attributed to the abrupt change in the total boson number or the density of the ground state at the transition point. Deep in the superfluid phase, on the other hand, the persistent current becomes independent of the gate voltage.

### B. Strongly coupled Josephson-junction necklaces

From the observation in Sec. III B, it is evident that in the strong-coupling limit the excitons such as particle-hole and particle-void pairs play dominant roles in the transport. In the picture of the lowest-order cotunneling processes illustrated in Fig. 12, however, such pairs are tightly bound throughout the transport process. Accordingly, the current induced in one necklace is accompanied by the secondary current in the other necklace, with the same magnitude but in the opposite direction.<sup>14</sup> On the other hand, in response to the magnetic flux, the charges in an excitonic pair tend to move in opposite directions since their signs are opposite (with respect to the offset charge  $n_g$ ). Therefore the current mirror effect competes with the influence of the magnetic flux.

Indeed, for small values of the Josephson energy ( $E_J/8E_0 \leq 0.07$ ), the persistent current is quite negligible both on the particle-hole symmetry line ( $n_g=0$ ) and on the maximal-frustration line ( $n_g=1/2$ ) (see Fig. 13). The small but still nonzero amount of persistent current is induced via higher-order tunneling processes. Namely, the charges in an excitonic pair break up, run down the circumferences in the opposite directions, and recombine. Contributions from these processes are observable only in a system with a small number of sites ( $N=8$  for the data in Fig. 13). In other words, the current mirror effect wins the competition. It is distinguished

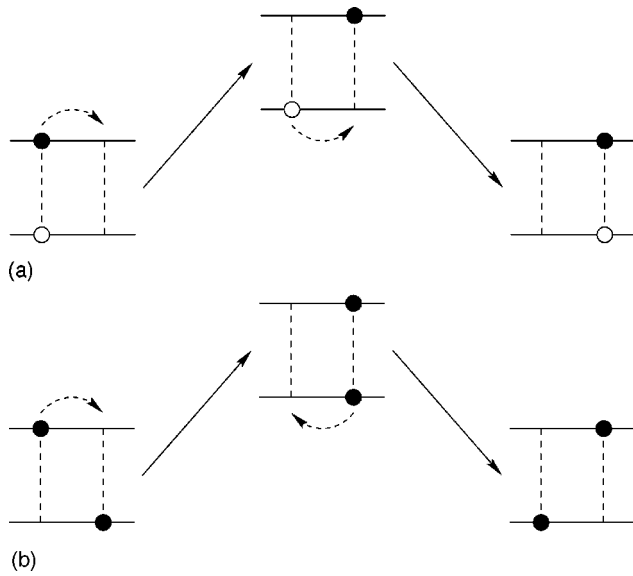


FIG. 12. Typical cotunneling processes relevant (a) near the particle-hole symmetry line and (b) near the maximal-frustration line. Such cotunneling results in current mirror effects.

from the behavior of the persistent current in a single Josephson-junction necklace, where for  $n_g=0$  the current increases rapidly near the transition point and any strength of the Josephson energy induces rather large persistent current for  $n_g=0.5$  (see Fig. 11), demonstrating the action of a different kind of charge fluctuations in the coupled system.

For larger values of the Josephson energy ( $E_J/8E_0 \geq 0.07$ ), however, a considerable amount of persistent current flows through the system and increases with  $E_J$ . It can be explained by the generation of excitations with higher charging energies in the presence of the Josephson energy. As observed in Fig. 8, with the increased Josephson energy, more of the charge states that do not satisfy  $n_x^+ = 0$  (near the particle-hole symmetry line) or  $n_x^+ = 1$  (near the maximal-frustration line) are now mixed with the lowest-charging-energy states. These excitations can carry a finite amount of persistent current since the signs of the charges in a pair are

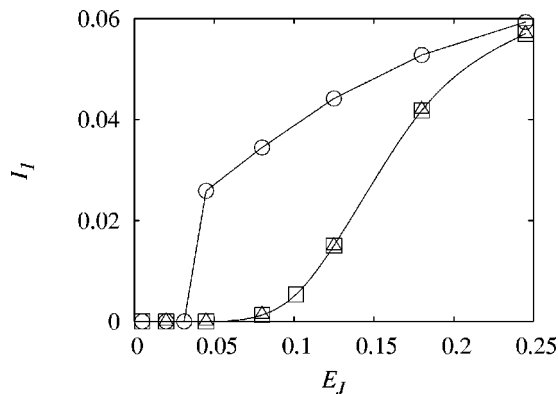


FIG. 13. Persistent current  $I_1$  (along one necklace) vs the Josephson energy  $E_J$  in the strongly coupled system of size  $N=8$ , for  $f=1/4$  and gate voltage  $n_g=0$  ( $\square$ ),  $0.2$  ( $\circ$ ), and  $0.5$  ( $\triangle$ ). Lines are merely guides to the eye.

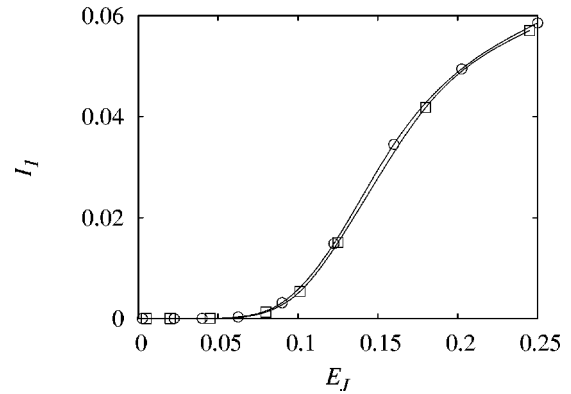


FIG. 14. Persistent current vs the Josephson energy on the particle-hole symmetry line ( $n_g=0$ ) in the strongly coupled system with the coupling capacitance  $C_1/C_0=100$  ( $\square$ ) and  $200$  ( $\circ$ ).

not opposite now. In short, magnetic frustration wins the competition with the current mirror effect. It is also interesting that the persistent currents for  $n_g=0$  ( $\square$ ) and  $1/2$  ( $\triangle$ ) are almost the same. In fact, the densities of charge excitations which do not satisfy the lowest-charging-energy condition are nearly the same for the two cases since the charging energy costs for such excitations amount to the same energy  $U_0$  in both cases.

Note also that unlike these two cases the persistent current for  $n_g=0.2$  ( $\circ$ ) increases sharply at the transition point and becomes quite larger than the one for  $n_g=0$  or  $1/2$ . Intermediate values of charge frustration (in the superfluid phase) bring about a variety of charge excitations in the presence of the Josephson energy and diminish the energy gap between the charge excitations, giving rise to a reduction of the current mirror effect and favoring independent single-charge transport.

Figure 14 shows that the persistent current increases slightly as the coupling capacitance is raised. On the one hand, a larger value of the coupling capacitance reduces the lowest excitation energy ( $\sim E_J$ ) and makes the excitons proliferate more in the system, thus increasing the persistent current due to the excitons. On the other hand, breaking of the excitons, which is crucial for inducing the persistent current, costs higher energy ( $\sim E_0$ ). These conflicting trends result in a slight increase in the regime of our interest ( $E_0 \gg E_J$ ).

The dependence of the current on the system size also supports our scheme for the role of the excitons in the persistent current. Figure 15 shows that, similarly to the case of a single necklace, in the insulating phase the current decays exponentially with system size and decreases inversely to the system size deep in the superfluid phase. Near the transition point on the side of the superfluid phase (at  $E_J/8E_0=0.08$  and  $0.125$ ), however, the current does display exponential dependence on the system size, which indicates that spatially localized objects participate in the generation of the current. It is another piece of evidence for the virtual processes of unpaired charges or higher-order excitons in the region where the low-lying excitons themselves are delocalized over the system.

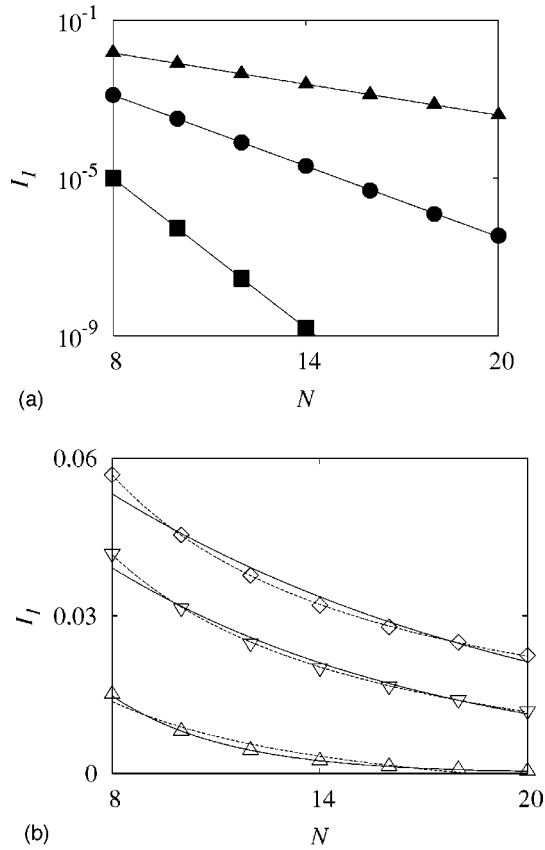


FIG. 15. Persistent current versus the system size on the particle-hole symmetry line ( $n_g=0$ ) for different values of the Josephson energy  $E_J=$  (a) 0.045 (▲), 0.08 (●), and 0.125 (▲); (b) 0.125 (Δ), 0.18 (∇), and 0.245 (◇) (again in units of  $8E_0$ ). The fitting curves are the same as those given in Fig. 10.

To reveal the cotunneling process more explicitly, we devise another interesting configuration that the magnetic field penetrates only one necklace ( $l=1$ ) without affecting the other ( $l=2$ ). Such a setup may be realized experimentally as shown in Fig. 16. Notice that only part of the two necklaces are capacitively connected. In order for the persistent current to flow through uncoupled grains, the Josephson coupling between those uncoupled grains should be sufficiently large. In this arrangement, one can observe the current mirror effect, similar to the case that only one chain is biased by an external voltage.<sup>13,15</sup>

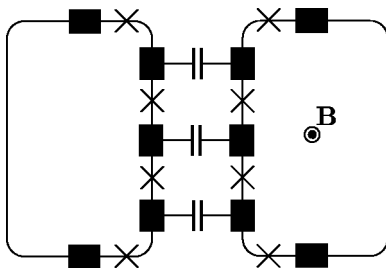


FIG. 16. Schematic diagram of two coupled Josephson-junction necklaces. Part of the two necklaces are capacitively connected whereas the magnetic field threads only one of the two necklaces.

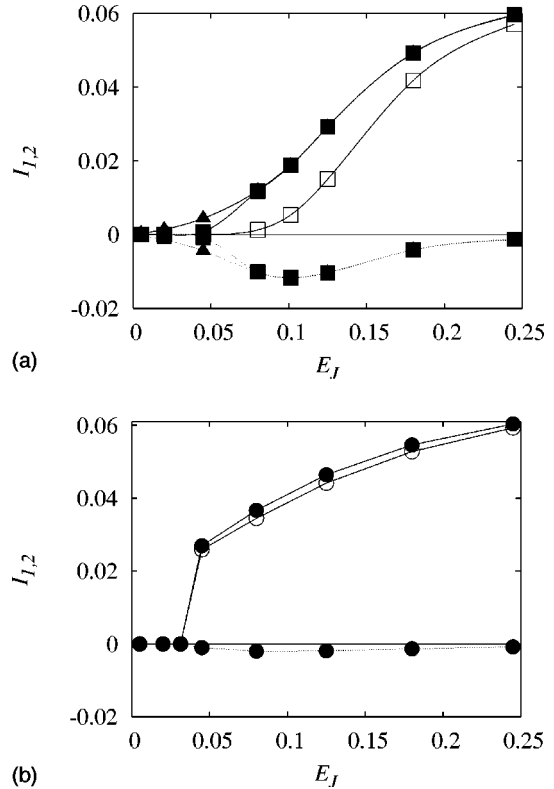


FIG. 17. Persistent currents  $I_1$  (solid lines with solid symbols) and  $I_2$  (dotted lines with solid symbols) when the magnetic field threads only the first ( $l=1$ ) necklace. The currents are calculated for the gate voltage  $n_g=$  (a) 0 (■), 0.5 (▲); (b) 0.2 (●). For comparison, the persistent currents when both the necklaces are threaded by the magnetic field (see Fig. 13) are also plotted, represented by the corresponding open symbols.

Figure 17(a) exhibits the current mirror effect in the system with the magnetic field threading only the first ( $l=1$ ) necklace. On the particle-hole symmetry and the maximal-frustration lines, the two persistent currents  $I_1$  and  $I_2$  along the first and second ( $l=2$ ) necklaces, respectively, satisfy the relation  $I_1 \approx -I_2$  in the range  $E_J/8E_0 \leq 0.07$ . As  $E_J$  is increased further, nonetheless, not only the mirror effect disappears gradually but also the current  $I_2$  diminishes to zero. It means that independent single-charge transport rather than the cotunneling transport is favorable at large values of the Josephson energy. Note that the current  $I_1$  is much higher than the corresponding current in the system with the magnetic field acting on both necklaces. Interestingly, unlike the previous setup, the persistent current for  $n_g=1/2$  is higher than that for  $n_g=0$ . Whereas on the maximal-frustration line the system is in the superfluid state of the particle-void pairs even at small  $E_J$ , on the particle-hole symmetry line a sufficient amount of the Josephson energy is necessary for generating excitons, i.e., particle-hole pairs. For  $n_g=0.2$ , the current mirror effect is indeed negligible and the increase in  $I_1$  is also very small, as shown in Fig. 17(b).

V. CONCLUSION

We have studied phase transitions and persistent currents in a ladder of two capacitively coupled Josephson-junction

necklaces. Emphasis has been placed on the roles of excitons in the presence of charge and magnetic frustration. To obtain the properties of the ground and excited states of the system, we have utilized the DMRG method for arbitrary values of the gate charge and magnetic flux. Although the main interest lies in the strong-coupling limit between the two necklaces, we have studied both the uncoupled and strongly coupled cases for comparison. In both cases, the gate voltage brings about crucial effects on the properties of the system. In a single Josephson-junction necklace, the presence of the gate voltage changes rather abruptly the behavior of the persistent current as well as nature of the phase transition. On the other hand, in the capacitively coupled Josephson-junction necklaces, such a drastic change is not observed but the gate voltage determines the class of excitons driving the phase transition: the particle-hole pairs near the particle-hole symmetry line and the particle-void pairs near the maximal-frustration line. In the presence of the Josephson tunneling, two different superfluid phases, characterized by the condensation of either of the two types of excitons, have been identified, depending on the gate charge. The pair correlation function and the exciton density have provided evidence for the formation of such excitons.

In the strongly coupled necklaces, the behavior of the

persistent current is manifested by the competition between the current mirror effect and magnetic frustration, which is associated with the cotunneling transport of the bound excitonic pairs of either particles and holes or particles and voids. At small values of the Josephson energy, the current mirror effect wins the competition and only a very small amount of persistent current is allowed for a finite-sized system. At large values of the Josephson energy, magnetic frustration can make use of higher-charging-energy states to dominate over the current mirror effect, allowing a considerable amount of persistent current. We have also suggested an experimentally realizable system to demonstrate the cotunneling process of the excitons. To our present knowledge, the only experimental work related to the system considered here is that reported in Ref. 15. Unfortunately, however, the large bias voltage applied to both arrays does not allow us to make a direct connection. In particular our DMRG algorithm is not suitable for such a nonequilibrium problem.

#### ACKNOWLEDGMENTS

We acknowledge partial support from the SKORE-A Program and from the BK21 Program.

\*Author to whom correspondences should be addressed. Electronic address: choims@korea.ac.kr

<sup>1</sup>See, e.g., *Single Charge Transport: Coulomb Blockade Phenomena in Nanostructures*, edited by H. Grabert and M. Devoret (Plenum Press, New York, 1992); D.V. Averin and K.K. Likharev, in *Mesoscopic Phenomena in Solids*, edited by B.L. Al'tshuler, P.A. Lee, and R.A. Webb (Elsevier Science, Amsterdam, 1991), p. 167.

<sup>2</sup>G. Schön and A.D. Zaikin, *Phys. Rep.* **198**, 237 (1990).

<sup>3</sup>M.Y. Choi, *Phys. Rev. B* **48**, 15920 (1993).

<sup>4</sup>R.M. Bradley and S. Doniach, *Phys. Rev. B* **30**, 1138 (1984); M.-S. Choi, J. Yi, M.Y. Choi, J. Choi, and S.-I. Lee, *ibid.* **57**, R716 (1998).

<sup>5</sup>R. Fazio and G. Schön, *Phys. Rev. B* **43**, 5307 (1991).

<sup>6</sup>A. van Otterlo, K.-H. Wagenblast, R. Fazio, and G. Schön, *Phys. Rev. B* **48**, 3316 (1993).

<sup>7</sup>*Macroscopic Quantum Phenomena and Coherence in Superconducting Networks*, edited by C. Giovannella and M. Tinkham (World Scientific, Singapore, 1995).

<sup>8</sup>B.J. Kim and M.Y. Choi, *Phys. Rev. B* **52**, 3624 (1995); **56**, 395 (1997).

<sup>9</sup>S. Sachdev, *Quantum Phase Transitions* (Cambridge University Press, Cambridge, England, 1999); see also cond-mat/9705266 (unpublished).

<sup>10</sup>*Mesoscopic Electron Transport*, edited by L.L. Sohn, L.P. Kouwenhoven, and G. Schön (Kluwer Academic, Dordrecht, 1997).

<sup>11</sup>In the literature, "particles" and "holes" are used mostly to refer to elementary excitations in fermion systems. In this paper, which is concerned with arrays of superconducting grains, we use them to refer to excess and deficit (bosonlike) Cooper pairs rather than constituent electrons.

<sup>12</sup>D.V. Averin, A.N. Korotkov, and Y.V. Nazarov, *Phys. Rev. Lett.* **66**, 2818 (1991).

<sup>13</sup>M. Matters, J.J. Versluys, and J.E. Mooij, *Phys. Rev. Lett.* **78**, 2469 (1997).

<sup>14</sup>M.-S. Choi, M.Y. Choi, T. Choi, and S.-I. Lee, *Phys. Rev. Lett.* **81**, 4240 (1998).

<sup>15</sup>H. Shimada and P. Delsing, *Phys. Rev. Lett.* **85**, 3253 (2000).

<sup>16</sup>E. Šimánek, *Inhomogeneous Superconductors: Granular and Quantum Effects* (Oxford University Press, New York, 1994), p. 54.

<sup>17</sup>R.A. Römer and M.E. Raikh, *Phys. Rev. B* **62**, 7045 (2000); J. Song and S.E. Ulloa, *ibid.* **63**, 125302 (2001); H. Hu, J.-L. Zhu, D.-J. Li, and J.-J. Xiong, *ibid.* **63**, 195307 (2001).

<sup>18</sup>S.R. White and R.M. Noack, *Phys. Rev. Lett.* **68**, 3487 (1992); S.R. White, *ibid.* **69**, 2863 (1992); *Phys. Rev. B* **48**, 10345 (1993).

<sup>19</sup>A. van Otterlo and K.-H. Wagenblast, *Phys. Rev. Lett.* **72**, 3598 (1994); A. van Otterlo, K.-H. Wagenblast, R. Baltin, C. Bruder, R. Fazio, and G. Schön, *Phys. Rev. B* **52**, 16176 (1995).

<sup>20</sup>T.D. Kühner, S.R. White, and H. Monien, *Phys. Rev. B* **61**, 12474 (2000).

<sup>21</sup>J.K. Freericks and H. Monien, *Europhys. Lett.* **26**, 545 (1994); *Phys. Rev. B* **53**, 2691 (1996).

<sup>22</sup>R. Baltin and K.-H. Wagenblast, *Europhys. Lett.* **39**, 7 (1997).

<sup>23</sup>V.L. Berezinskii, *Zh. Eksp. Teor. Fiz.* **59**, 907 (1970) [*Sov. Phys. JETP* **32**, 493 (1971)]; J.M. Kosterlitz and D.J. Thouless, *J. Phys. C* **6**, 1181 (1973); J.M. Kosterlitz, *ibid.* **7**, 1047 (1974); J.V. José, L.P. Kadanoff, S. Kirkpatrick, and D.R. Nelson, *Phys. Rev. B* **16**, 1217 (1977).

<sup>24</sup>M.Y. Choi, S.W. Rhee, M. Lee, and J. Choi, *Phys. Rev. B* **63**, 094516 (2001).

<sup>25</sup>M.-S. Choi, M.Y. Choi, and S.-I. Lee, *J. Phys.: Condens. Matter* **12**, 943 (2000).

<sup>26</sup>M.Y. Choi and M. Lee, *Curr. Appl. Phys.* **2**, 11 (2002).